Photoionization of endohedral atoms: Molecular and interchannel-coupling effects

A. Ponzi, P. Decleva, and S. T. Manson

Phys. Rev. A **92**, 023405 — Published 10 August 2015

DOI: 10.1103/PhysRevA.92.023405

PHOTOIONIZATION OF ENDOHEDRAL ATOMS: MOLECULAR AND INTERCHANNEL COUPLING EFFECTS

A. Ponzi, P. Decleva

Dipartimento di Scienze Chimiche, Universita' di Trieste, Via Giorgieri 1, I-34127 Trieste, Italy and CNR IOM, Trieste, Italy

S. T. Manson

Department of Physics and Astronomy, Georgia State University, Atlanta, Georgia 30303, USA

Abstract

Calculations of the photoionization cross section of the 2*p* and 3s subshells of free Ar and Ar@C_{60} as an example have been performed using the molecular structure of the confined system and time-dependent density functional theory (TDDFT) for the dynamical quantities. The results for Ar 2p in the combined system exhibit significant confinement resonances with the lower–energy ones being quite sharp, in contrast to the results a jellium-model calculations. In addition, calculations done with and without interchannel coupling between the photoionization channels of the 2*p* of the Ar atom and the 1*s* of the C_{60} shell shown that, in this case, the coupling is of negligible importance, even though the C 1s cross section is more than an order of magnitude larger that Ar 2*p* in the 300 eV range. The Ar 3s, which is not hybridized, also exhibits confinement resonances, but is very strongly affected by interchannel coupling with photoionization channels from the C60 shell. The phenomenology of both 2p and 3s is explained in terms of the interchannel coupling matrix elements. These results should be applicable to inner-shell ionization of essentially any endohedral fullerene system.

I. Introduction

Over the past decade or so there have been a large number of studies of the photoionization of endohedral atoms—atoms confined in a fullerene or other type of cage [1-14]. These investigations were stimulated by the fact that endohedral atoms are of both basic and applied interest. On the basic side, they present an exceptionally clean and stable "laboratory" to study the effects of confinement upon the properties on the encapsulated atom; to understand how the confinement alters the static and dynamic properties of the atom. In addition, many possible applications of endohedral atoms include quantum computing [15], drug delivery [16], photovoltaics [17] and hydrogen storage [18], among others.

Of the many extant photoionization studies, the overwhelming majority are theoretical, owing to the difficulties in the fabrication of endohedral systems in large enough quantities to investigate experimentally, although some experimental photoionization work has been reported [10]. Furthermore, almost all of the theoretical investigations have treated the potential of the confining shell in a spherical jellium model of one sort or another [18, 10-13,20]. The few studies considering the full molecular potential have been at the DFT (static mean-field) [19] or static-exchange (Hartree-Fock) level [9]. Thus, there are no reports of calculations which include both molecular structure and correlation; such calculations are, however, important to provide some notion of the qualitative and quantitative accuracy of the previous calculations. This is needed owing to the relative scarcity of experimental results.

To ameliorate the situation, we have embarked upon a program to do just that, to perform calculations of the photoionization of confined atoms including both the molecular structure of the target and correlation. The correlation is included through the use of time-dependent density functional theory (TDDFT) [21,22] which is an outgrowth of earlier work at just the DFT [19] level. As a first step we have chosen Ar@C_{60} which has been the subject of a number of earlier studies [1,2,4, 9,11,23-28]. There are two questions which we are particularly interested in: how confinement resonances are affected by the inclusion and interaction of both the molecular structure and correlation; and how the inclusion of the C 1*s* channels of C_{60}, and the interchannel coupling with these channels, affects the inner-shell atomic photoionization channels. We consider the Ar 2*p* and 3*s* cross sections to explore these questions, but the results should be generally applicable to any endohedral fullerene. Ar 2*p* and 3*s* were chosen because they are inner shells (no hybridization and negligible interaction with the confining shell) [27,29] so that we could focus on the effect(s) of the confining environment and correlation on the final state continuum wave function which results in the changes to the cross section. These are important questions. Confinement resonances in any confined system gives significant information about the physical dimensions and shape of the confining shell [2]. And an understanding of the effect(s) of the C 1*s* ionization channels of the C_{60} fullerene on the inner-shell ionization of the caged atom should be widely applicable to any atom trapped in any fullerene cage.

The following section gives a brief presentation of the theoretical methodology. In Sec. III, the results of the calculations are presented and discussed. The final section includes a summary, conclusions and some prospectus as to where we go from here.

II. Brief Description of the Theoretical Methodology

The computational approach used in our research has been described in detail in previous work [30-32] and has been shown to produce results in excellent agreement with the experiment; here we limit the discussion to a summary of only the main steps. The method is based on accurate solution of the scattering problem in a Density Functional Theory (DFT) framework and utilizes a discretization of both bound and continuum wave functions in a multicenter basis of B-spline functions, B_i, times real spherical harmonics $Y_{lm}(\theta,\varphi)$

$$\chi_{ilm} = 1/r\ B_i(r)\ Y_{lm}(\theta,\varphi)$$

which are further fully adapted to the molecular symmetry. The bound states are calculated by a conventional generalized diagonalization of the Kohn-Sham Hamiltonian matrix while the continuum states are obtained by a least squares approach. The self-consistent-field (SCF) initial electronic density of the ground state is first obtained by a standard LCAO approach utilizing the ADF program [33,34]. The exchange-correlation potential LB94 [35] is employed, with a double-zeta with polarization (DZP) basis set for Ar and C taken from the optimized database included in the ADF package. From the ground state density, a fixed Kohn-Sham Hamiltonian is obtained and it is further diagonalized in the B-spline basis both for the bound and continuum states (static-exchange DFT approach). The B-spline basis set comprises a long range expansion around a common origin (one-center expansion), with large angular momenta, to describe the continuum wave functions up to the asymptotic Coulomb region, where they are fitted to analytical solutions, and a set of additional functions centered on the various nuclei, in the spirit of the LCAO approach, which take care of the Coulomb singularities at the nuclei, and ensure rapid convergence of the expansion. In the present calculation an interval up to R_{max}= 25 atomic units (au) has been employed for the one-center expansion, with a step size of 0.2 au, and maximum angular momentum up to L_{max}= 25. For the expansions around the carbon atoms L_{max}= 2 was employed. The radial expansions around the carbon atoms were R_{max}= 1.32 au. These choices ensured complete convergence of the calculated cross sections reported.

Cross sections and asymmetry parameters can finally be obtained by the calculation of transition dipole moments, through standard angular momentum analysis [36]. For the TDDFT calculations, we employed the non-iterative algorithm previously developed [32]. The basic dynamical variable becomes linear response potential $V^{SCF} = V^{ext} + \delta V$. This, as well as the

wave functions, is expanded in the full multicenter B-spline basis, and all equations are recast as matrix equations: both

$$\delta\rho = \chi\, V^{SCF} \quad \text{and} \quad \delta V = K\, \delta\rho$$

are linear, define χ and K matrices, the linear susceptibility χ and the kernel K that gives the potential generated by a charge density change $\delta\rho$. Combining we arrive at the equation for V^{SCF}

$$(K\chi - 1)\, V^{SCF} = V^{ext}$$

The computationally most demanding part is the evaluation of the χ matrix, which is energy-dependent and has to be recomputed at each selected energy. It is obtained by first order time dependent perturbation theory. Finally the TDDFT transition matrix elements are obtained by substituting V^{SCF} in place of the dipole operator V^{ext} in the transition dipole matrix elements,

$$d^{(-)}_{Elm,\gamma,i} = < \varphi^{(-)}_{Elm} \mid V^{SCF}{}_{\gamma} \mid \varphi_i >$$

where φ_i and $\varphi^{(-)}_{Elm}$ are the initial and final (incoming wave boundary conditions) wave functions of the system, and γ represents the photon polarization.

III. Results and Discussion

The results of our calculations for the 2*p* subshell of free Ar and confined Ar@C_{60} are given in Fig. 1; in the confined case, in molecular notation, Ar 2*p* becomes the 3T1u state of the combined Ar@C_{60} system. For the free case, the DFT cross section exhibits a small rise from threshold resulting from the shape resonance in the d-wave continuum of the $2p \rightarrow \varepsilon d$ transition. Including correlation with the TDDFT result, the shape resonances are still there, although somewhat altered in shape from DFT, and a significant difference in magnitude is seen at threshold, a difference which decreases with increasing energy, eventually disappearing completely. This difference arises from both initial state correlation (configuration interaction with double excitations), and final state correlation (in the form of interchannel coupling among photoionization channels) [37]. It is of importance to point out that the present TDDFT results are in excellent agreement with experiment and previous sophisticated calculations (not shown) [38]. This agreement is of importance because it shows that the present TDDFT calculation includes all of the important atomic effects for this particular case. It is also to be noted that the cross sections, except for the near-threshold shape resonance, are quite smooth as a function of energy.

Looking now at the confined case, a rather different picture emerges. The atomic cross section is very substantially modulated; these modulations are known as confinement resonances [39] and have been seen experimentally for the case of 4*d* photoionization in the Xe@C_{60}

endohedral fullerene [10]. Basically these are caused by interference between the photoelectron wave emerging directly with waves that are scattered from the inner and outer walls of the confining C_{60} shell [39,40]. It is important to note that these confinement resonances are almost exactly the same in DFT and TDDFT calculations, thereby confirming that confinement geometry is the dominant determinant of this phenomenon; correlation, although it is seen to have some effect, does not play a large role in their behavior, i.e., the confinement resonances are determined almost solely by confinement geometry.

Note also that the three lowest resonances closest to threshold are quite sharp, but the higher energy resonances are much smoother. The sharpness of the resonances near threshold is evidently due to the more granular nature of the confinement potential when the molecular structure is considered; the slower photoelectrons have more time to "experience" the different confinement potential. This is rather different than the predictions of a spherical jellium model of the confining potential which predicts all confinement resonances to be rather smooth [11]. However, it does agree with a previous study at the Hartree-Fock level which also predicted sharp near-threshold confinement resonances [9]. The confinement resonances are also stronger than those predicted by a spherical jellium model of the confining potential [11]; even 150 eV above threshold, the amplitude is about 10 % of the cross section. The amplitude of the confinement resonances diminish much more rapidly with energy in a jellium model. This difference too is evidently the effect of using the full molecular, as opposed to jellium, confining potential in the calculations. In general, it is expected that deficiencies of the jellium model stems from the excessive delocalization of the valence electron charge (typically 240 electrons) compared with a full molecular calculation. In the latter, electrons are more tightly bound close to the carbon atoms, and to the C-C bonds. So scattering of the photoelectrons from the hard atomic cores is significantly enhanced; and, on the other hand, response effects are diminished, due to the lower mobility of the electron cloud.

The sharpness of the lower-energy confinement resonances would probably not be seen in a room temperature experiment owing to the vibrations which would move some of the confined atoms off-center, thereby smearing out the confinement resonances. Such a mechanism was suggested earlier as an explanation as to why confinement resonances had not been seen; they have since been observed [41]. This suggests that, to compare with experiment, a broadening factor would have to be applied to account for this vibrational excitation. This also suggests that experimental work on cold target systems would change the observed shape of the low-energy near-threshold confinement resonances.

Now, in the results presented in Fig. 1, the Ar 2*p* photoionization channels for the confined system were not coupled to the C 1*s* photoionization channels arising for the C_{60} cage, which were kept frozen. This could be of some importance since the C 1s threshold is at about 300 eV, so that above 300 eV the Ar 2*p* and C 1*s* photoionization channels are both open; furthermore, the threshold C_{60} 1*s* photoionization cross section is about 100 Mb, which is estimated normalizing experimental results at higher energy as 60 times the cross section of the

free carbon atom [42], and this is more than an order of magnitude larger than the Ar 2*p* cross section at that energy, as seen in Fig. 1. Thus, with a small mixing of the C_{60} 1s cross section, the Ar 2*p* cross section could be considerably altered. To explore this possibility, the calculation for the confined system has been redone at the TDDFT to include interchannel coupling with C 1*s*; the Ar 2*p* photoionization cross sections are shown in Fig. 2, with and without the interchannel coupling between Ar 2*p* and C1*s*. The outstanding feature of this comparison is that the curves are almost exactly the same; thus, despite the C 1*s* cross section being about a factor of ten larger than the Ar 2*p* cross section around 300 eV, the interchannel coupling is negligible. The same can be said about the absence of autoionization resonances due to the huge C1s $\rightarrow$ C2p π^* below threshold excitation. In fact similar coupling of core excitations on one site with another site ionization was expected and first reported (so called MARPE effect) in solid state photoemission [43], but it proved elusive afterwards, and has been barely detected in isolated molecules [44].

To understand this result, it is important to note that two conditions must be fulfilled for interchannel coupling to alter a cross section of a particular photoionization channel. First, the cross section for that channel must be degenerate with a channel with a significantly larger cross section. And second, there must be a non-negligible interchannel coupling matrix element connection the two channels [37]. The first condition is clearly satisfied for Ar 2*p* with C_{60} 1*s*, as discussed above. Thus, given the results depicted in fig. 2, it must be the case that the interchannel coupling matrix elements are extremely small. The direct part of the matrix element for this case, the Coulomb interaction between the $2p^5\varepsilon l1s^{60}$ final state and the $2p^61s^{59}\varepsilon\square\, l\square$ final state (2*p* is Ar 2*p* and 1*s* is C_{60} 1*s*), can be written as $< 2p\varepsilon l|\frac{1}{r_{12}}|\varepsilon' l' 1s >$, and is included in the calculation. This coupling matrix element is, however, negligible because each of the discrete orbitals in the direct matrix element overlaps with the continuum orbital of the other channel. Even at the C 1*s* threshold, where the exchange matrix element should maximize, while the $\varepsilon\square\, l\square$ continuum orbital (arising from C 1s ionization) is slowly varying, the εl orbital, arising from Ar 2*p* ionization moderately energetic and oscillates rather rapidly. Thus, while the 2*p* overlaps somewhat with the threshold $\varepsilon\square\, l\square$ function, the overlap of the 1s with the εl orbital is negligible, owing to the oscillation in the latter. And this matrix element clearly decreases rapidly with increasing energy because the continuum wave functions oscillate more rapidly in space as the energy increases so that the overlap with the discrete wave functions decreases. The exchange part of the interchannel coupling matrix element, $< 2p\varepsilon l\left|\frac{1}{r_{12}}\right| 1s\varepsilon' l' >$, is treated only approximately in LDA, substituting the derivative of the exchange-correlation potential, V_{XC}, in place of the coulomb operator $1/r_{12}$, so that the exchange matrix element is calculated as . $< 2p\varepsilon l|\ \partial V_{XC}/\partial r|1s\varepsilon' l' >$. This matrix element too is quite small in the present case because the overlap of the discrete Ar 2*p* and C 1*s* wave functions is so small because these two wave functions are quite compact (~0.2 atomic units in radius) and centered about 6 au apart. Since this exchange matrix element is negligible, in the present case, it is evident that the approximation here causes no inaccuracies. Furthermore, it is indeed a general feature that core

ionizations arising from different inequivalent sites of the same atomic species, e.g. C1s ionization from inequivalent molecular sites, are very weakly coupled, and that is generally borne out in TDDFT calculations. On the other hand, the inadequacy of the TDDFT exchange matrix elements to describe charge transfer excitation between spatially separated sites, due to the exponential compared to coulombic decay of the exchange matrix element has been documented in the literature [45,46]

This understanding suggests that it might be possible for interchannel coupling to be important if the confined atom or molecule has an inner subshell whose ionization energy was very close to the C 1s ionization energy, in which case, interchannel coupling in the threshold region could be significant, owing to the exchange part of the interchannel coupling matrix element. A molecule containing a carbon atom is a good candidate for this since the 1*s* electrons of the carbon in the confined molecule will have a threshold energy very close to the1*s* of the carbon atoms of the C_{60} shell.

Next consider the Ar 3s subshell which has the same symmetry as the 2Ag level of free C_{60} so they are considered together. The same problem hase been recently considered by Jose and Lucchese [9], at the static-exchange level. In Fig. 3, the DFT and TDDFT results for the photoionization cross sections of free Ar 3s and the 2Ag state of free C_{60} are shown. The Ar 3s DFT cross section is quite smooth and similar to the HF one [9], but the addition of interchannel coupling through the TDDFT calculation induces a Cooper minimum and a completely different spectral shape in the threshold region, in excellent agreement with experiment and previous theoretical work [47]. Note that, above about 70 eV, where interchannel coupling with the Ar 3p ionization channels becomes unimportant, the DFT and the TDDFT are essentially the same. For the 2Ag state of Free C_{60}, the DFT result is seen to exhibit confinement resonances and is quite similar to the Hartree-Fock (HF) result [9]. The introduction of correlation through the TDDFT calculation induces some changes in the 2Ag cross section over most of the energy range; the confinement resonance at about 40 eV is increased by about 50%. The region very close to threshold is changed markedly, however, owing to the autoionizing resonances.

Going now to Ar@C_{60}, the situation changes dramatically. The cross sections for the 4Ag state in Ar@C_{60}, essentially the Ar 3s (which is not hybridized), and the 5Ag is what the 2Ag of free C_{60} becomes in the combined system, as shown in Fig. 4. To begin with, note that the reverse ordering is obtained at the HF level [9], with the two levels almost degenerate. It is hard to speculate on the exact ordering in the absence of more accurate calculations, which is, in any case, not very relevant for the present discussion, except noting that both calculations agree in finding no hybridization between Ar3s and C_{60} orbitals, despite the closeness in energy of the two levels. Most important, however, is that the 4Ag (3s) cross section is virtually unrecognizable from the free case. The DFT result shows a cross section which displays a number of confinement resonances owing to the confinement; this result is qualitative similar to the earlier HF result [9]. This occurs even though the initial state, the Ar 3s, remains virtually unaltered by the confinement since it is not hybridized, the final continuum state is significantly

altered by the molecular potential of the C_{60} cage.. The confinement resonances are part and parcel of the effect of the C_{60} on the continuum wave function.

However, looking at the TDDFT cross section, it is clear that interchannel coupling engenders significant changes in the 4Ag (3s) cross section, particular at the lower energies; the prominent confinement resonance at about 45 eV is reduced in magnitude by a factor of five or so by the coupling. This could be also tied to the Cooper minimum in free Ar, caused by interchannel coupling and properly included at the TDDFT level. At the higher energies, however, the effects of the coupling die out and the DFT and the TDDFT results are virtually identical. To understand this phenomenology, note that the interchannel coupling matrix element where the Ar 3s wave function overlaps with a discrete wave function of the C_{60} cage is negligible because the overlap is negligible. On the other hand, since the binding energy of Ar 3s is quite close to the binding energy of a number of C_{60} shell orbitals, the interchannel coupling matrix elements where each discrete orbital overlaps with a continuum orbital is not small because the continuum orbitals, both being near threshold, oscillate only very slowly with r. With increasing energy, however, they oscillate more rapidly, thereby "killing" the interchannel coupling matrix element. This explains why there is significant interchannel coupling near threshold, but essentially none above about 70 eV, as seen in Fig. 4. These results are qualitatively similar to what was found in calculations using a jellium model to approximate the molecular potential of the fullerene cage [11,23].

The 5Ag cross section, essentially a pure C_{60} state, behaves somewhat differently. The DFT cross section is quite similar to the cross section for the 2Ag of free C_{60}, although there are some differences which reflect the fact that the molecular field changes somewhat owing to the introduction of the endohedral Ar atom. At the TDDFT level, significant alteration is evident at the lower energies, particularly around 45 eV, for the same reasons as discussed above in connection with the 4Ag (3s) cross section. At the higher energies, however, there remain effects of interchannel coupling, like the roughly 30 % increase in the confinement resonate at 70 eV. This is because the 5Ag orbital, being a C_{60} orbital, overlaps reasonably well with other C_{60} orbitals so that the interchannel coupling matrix elements where the discrete orbital overlap is not negligible as it was in the case of the 4Ag (3s) overlap. Thus, while interchannel coupling between the 4Ag (3s) photoionization channel and the C_{60} channels is essentially gone at 70 eV, this is not the case for 5Ag, since it is a C_{60} orbital itself.

IV. Summary and Conclusions

The first calculation of the photoionization of an atom confined in a fullerene cage taking both correlation and molecular structure has been performed. The Ar@C_{60} system was investigated and the near-threshold confinement resonances were found to be quite sharp, unlike the findings of calculation using spherical jellium models of the confining potential [1-8]. In addition, as a result of the inclusion of molecular structure, the confinement resonances were found to extend to much higher energy as compared to jellium calculation [1-8]. Furthermore, it

was found that correlation has only very minor effects on the confinement resonances which means that they are determined largely by the detailed structure of the confining system, a very general result. This also means that experimental observation of confinement resonances provides information on confinement geometry, including where the trapped atom or molecule resides in the confinement cavity.

It was also seen that interchannel coupling of the small Ar 2*p* photoionization cross section with the (degenerate) much large C_{60} 1*s* channels was not found, and the finding explained. As a result of the understanding of why interchannel coupling was negligible in this case, it was also suggested under what conditions interchannel coupling between the C_{60} 1*s* and the photoionization channels of a confined atom or molecule might be found. However, it is evident that this is a general result; interchannel coupling in the photoionization of essentially any inner subshell of any atom confined in a fullerene will be negligible. This new understanding is of importance in that theoretical studies of inner-shell ionization has been avoided in the past because the conventional wisdom was that in the energy neighborhood of the very large C 1*s* cross section of the fullerene shell, the atomic cross section would be greatly affected by interchannel coupling, and no previous calculation include this coupling. Thus, the present results open the door to a number of new studies that were hitherto avoided. It should also be mentioned that inner-shell ionization investigations of confined atoms are particularly useful in that the initial states, being so compact, are essentially entirely atomic so that all the changes from the free atom cross sections result from confinement effects on the final continuum state wave functions, i.e., inner-shell ionization studies of confined atoms amounts to spectroscopy of the continuum wave functions.

In addition, our study of the photoionization of Ar 3s, and the related C_{60} 2Ag, in the Ar@C_{60} system has revealed both significant effects of the molecular potential along with significant interchannel coupling. Even though Ar 3s is still an inner shell and not hybridized, still interchannel coupling has a large effect on the cross section in the threshold region, an effect that gradually disappears with increasing energy; this behavior was explained in terms of the details if the interchannel coupling matrix element. Investigation of the 5Ag cross section (which is essentially the C_{60} 2Ag in the combined system) revealed a somewhat different phenomenology. This cross section is perturbed only a small amount from the free C60 case owing to the introduction of the Ar atom. In the threshold region, here too, extensive alteration of the cross section was found, and these alterations, while they decreased with increasing energy, decreased much less rapidly than in the 3s case for reasons explained.

As far as future work is concerned, we have begun investigating the photoionization of all of the subshells of the encapsulated Ar atom with an eye to understanding where the simpler jellium results are correct and where they need correction. Based upon that investigation, other systems will be scrutinized. In addition, the influence of the vibrational motion on the damping of the resonances will be investigated.

Finally, by producing cross section of significant accuracy, it is our hope that these and future results will stimulate laboratory investigations of the photoionization of endohedral fullerenes. And with the increasing capabilities of fabricating significant quantities of samples, we urge that photoelectron spectroscopic studies be performed to separate the cross section by subshell and test theory stringently.

Acknowledgments

PD gratefully acknowledges support from the European COST Action CM1204 XLIC. STM is grateful for support from the US Department of Energy, Office of Chemical Sciences under grant DE-FG02-03ER15428.

References

[1] V. K. Dolmatov, A. S. Baltenkov, J.-P. Connerade, and S. T. Manson, Radiat. Phys. Chem. **70**, 417 (2004) and references therin.
[2] V. K. Dolmatov, in *Advances in Quantum Chemistry: Theory of Quantum Confined Systems*, edited by J. R. Sabin and E. Brandas (Academic, New York, 2009), pp. 13–68 and references therein.
[3] J.-P. Connerade, in *The Fourth International Symposium on Atomic Cluster Collisions: Structure and Dynamics from the Nuclear to the Biological Scale*, edited by A. V. Solovyev and E. Surdutovich, AIP Conf. Proc. No. 1157 (AIP, New York, 2009), pp. 1–33 and references therein.
[4] H. S. Chakraborty, M. A. McCune, M. E. Madjet, D. E. Hopper and S. T. Manson, in *The Fourth International Symposium on Atomic Cluster Collisions: Structure and Dynamics from the Nuclear to the Biological Scale*, edited by A. V. Solovyev and E. Surdutovich, AIP Conf. Proc. No. 1157 (AIP, New York, 2009), pp. 111–118 and references therein.
[5] M. E. Madjet, T. Renger, D. E. Hopper, M. A. McCune, H. S. Chakraborty, Jan-M. Rost and S. T. Manson, Phys. Rev. A **81**, 013202 (2010).
[6] B. Li, G. O'Sullivan and C. Dung, J. Phys. B **46,** 155203 (2013).
[7] T. W. Gorczyca, T.-G. Lee and M. Pindzola, J. Phys. B **46**, 195201 (2013).
[8] M. Ya. Amusia, Chem. Phys. **414**, 168 (2013) and references therein.
[9] J. Jose and R. Lucchese, J. Phys. B **46**, 215103 (2013).
[10] R. A. Phaneuf, A. L. D. Kilcoyne, N. B. Aryal, K. K. Baral, D. A. Esteves-Macaluso, C. M. Thomas, J. Hellhund, R. Lomsadze, T. W. Gorczyca, C. P. Ballance, S. T. Manson, M. F. Hasoglu, S. Schippers, and A. Müller, Phys. Rev. A **88**, 053402 (2013) and references therein.
[11] M. H. Javani**,** H. S. Chakraborty, and S. T. Manson, Phys. Rev. A **89**, 053402 (2014).
[12] P. C. Deshmukh, A. Mandal, S. Saha, A. S. Kheifets, V. K. Dolmatov and S T Manson, Phys. Rev. A **89**, 053424 (2014) and references therein.
[13] M. H. Javani, R. De, M. E. Madjet, S. T. Manson and H. S. Chakraborty, J. Phys. B **47,** 175102 (2014).
[14] Z. Chen and A. Z Msezane, Phys. Rev. A **89**, 025401 (2014) and references therein.
[15] W. Harneit, C. Boehme, S. Schaefer, K. Huebener, K. Fostiropoulos, and K. Lips, Phys. Rev. Lett. **98**, 216601 (2007).
[16] J. B. Melanko, M. E. Pearce, and A. K. Salem, in *Nanotechnology in Drug Delivery*, edited by M. M. de Villiers, P. Aramwit, and G. S. Kwon (Springer, New York, 2009), p. 105.
[17] R. B. Ross, C. M. Cardona, D. M. Guldi, S. G. Sankaranarayanan, M. O. Reese, N. Kopidakis, J. Peet, B.Walker, G. C. Bazan, E. V. Keuren, B. C. Holloway, and M. Drees, Nat. Mater. **8**, 208 (2009).
[18] Y. Zhao, Y.-H. Kim, A. C. Dillon, M. J. Heben, and S. B. Zhang, Phys. Rev. Lett. **94**, 155504 (2005).
[19] M. Stener, G. Fronzoni, D. Toffoli, P. Colavita, S. Furlan, and P. Decleva, J. Phys. B **35**, 1421 (2002) and references therein.
[20] Y. B. Xu, M. Q. Tan, and U. Becker, Phys. Rev. Lett. **76**, 3538 (1996).
[21] E. Runge and E. K. U. Gross, Phys. Rev. Lett. **52**, 997 (1984).
[22] E. K. U. Gross and W. Kohn, Phys. Rev. Lett. **55**, 2850 (1985).
[23] M. E. Madjet, H. S. Chakraborty, and S. T. Manson, Phys. Rev. Lett. **99**, 243003 (2007).

[24] M. Ya. Amusia, A. S. Baltekov and L. V. Cernycheva, JETP **107**, 180 (2008).
[25] V. K. Dolmatov, P. Brewer and S. T. Manson, Phys. Rev. A **78**, 013415 (2008).
[26] M. Ya. Amusia, A. S. Baltekov and L. V. Cernycheva, J. Phys. B **41**, 165201 (2008).
[27] M. Morscher, A. P. Seitsonen, S. Ito, H. Takagi, N. Dragoe and T. Greber, Phys. Rev. A **82**, 051201(R) (2010).
[28] M. H. Javani, J. B. Wise, R. De, M. E. Madjet, S. T. Manson and H. S. Chakraborty, Phys. Rev. A **89**, 063420 (2014).
[29] H. S. Chakraborty, M. E. Madjet, T. Renger, Jan-M. Rost and S. T. Manson, Phys. Rev. A **79**, 061201(R) (2009).
[30] H. Bachau, E. Cormier, P. Decleva, J. E. Hansen, and F. Martín, Rep. Prog. Phys. **64**, 1815 (2001).
[31] D. Toffoli, M. Stener, G. Fronzoni, and P. Decleva, Chem. Phys. **276**, 25 (2002).
[32] M. Stener, G. Fronzoni, and P. Decleva, J. Chem. Phys. **122**, 234301 (2005).
[33] G. te Velde, F.M. Bickelhaupt, S.J.A. van Gisbergen, C. Fonseca Guerra, E.J. Baerends, J.G. Snijders and T. Ziegler, *Chemistry with ADF*, J. Comput. Chem. 22, 931 (2001)
[34] E.J. Baerends et al, ADF2014, SCM, Theoretical Chemistry, Vrije Universiteit, Amsterdam, The Netherlands, http://www.scm.com.
[35] R. van Leeuwen and E. J. Baerends, Phys. Rev. A **49**, 2421 (1994).
[36] N. Chandra, J. Phys. B **20**, 3405 (1987).
[37] U. Fano and J. W. Cooper, Rev. Mod. Phys. **41**, 441 (1968).
[38] D. W. Lindle, L. J. Medhurst, T. A. Ferrett, P. A. Heimann, M. N. Piancastelli, S. H. Liu, D. A. Shirley, T. A. Carlson, P. C. Deshmukh, G. Nasreen and S. T. Manson, Phys Rev. A **38**, 2371 (1988) and references therein.
[39] J.-P. Connerade, V. K. Dolmatov and S. T. Manson, J. Phys B **33**, 2279 (2000).
[40] P. C. Deshmukh, A. Mandal, S. Saha, A. S. Kheifets, V. K. Dolmatov and S T Manson, Phys. Rev. A **89**, 053424 (2014).
[41] A. V. Korol and A. V. Solovyov, J. Phys B **43**, 201004 (2010).
[42] J. Berkowitz, J. Chem. Phys. **111**, 1446 (1999).
[43] A. Kay, E. Arenholz, S. Mun, F. J. Garcia de Abajo, C. S. Fadley, R. Denecke, Z. Hussain, M. A. Van Hove, Science **281**, 679 (1988).
[44] M. Yamazaki, J. Adachi, T. Teramoto and A. Yagishita, J. Phys. B **46**, 115101 (2013).
[45] A. Dreuw, J. L. Weisman, and M. Head-Gordon, J. Chem. Phys. **119**, 2943 (2003).
[46] O. Gritsenko and E. J. Baerends, J. Chem. Phys. **121**, 655 (2004).
[47] A. F. Starace in *Handbuch der Physik,* Vol. 31, edited by W, Mehlhorn (Springer-Verlag, Berlin, 1982), pp. 1-121.

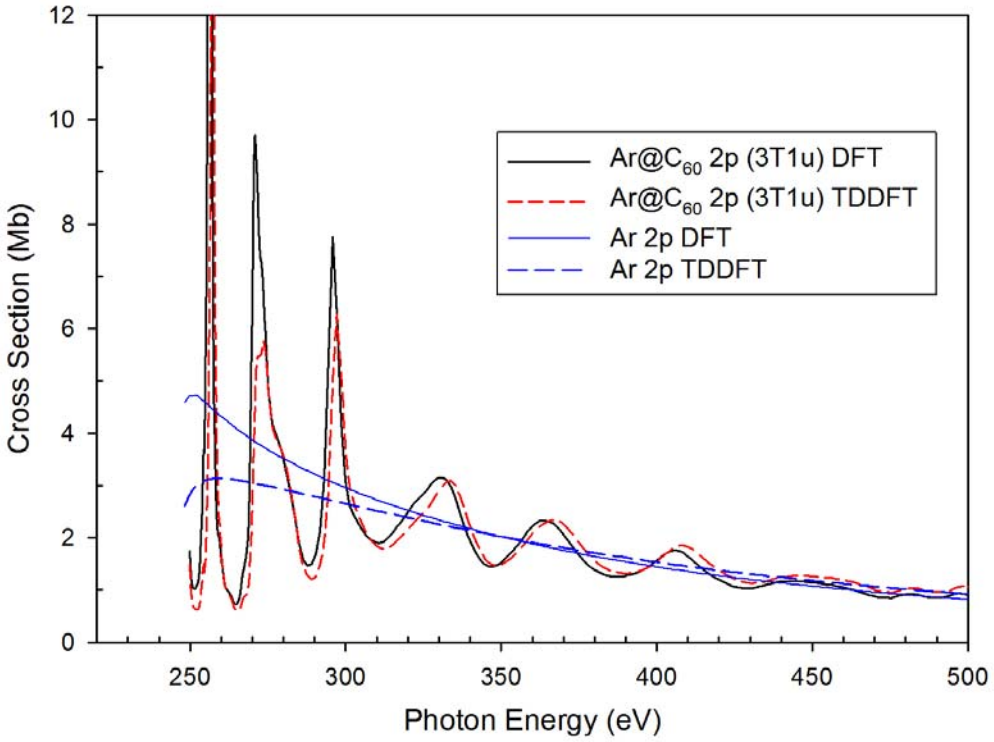

Fig. 1. (color online) Photoionization cross section for the free and confined Ar 2*p* subshell each calculated using DFT and TDDFT methods without coupling to the C 1*s* channels of the C_{60} shell.

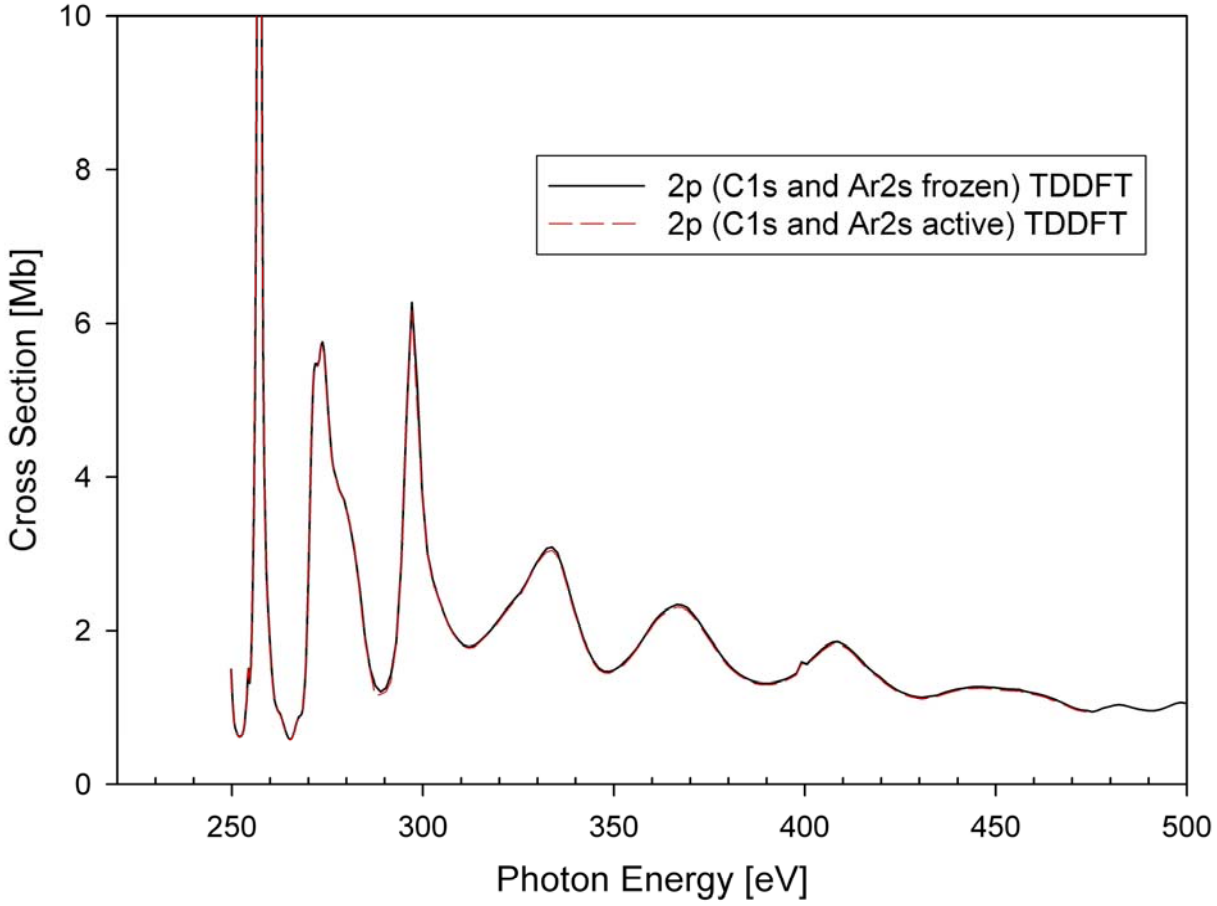

Fig. 2: (color online) Calculated photoionization cross section for confined Ar 2*p* at the TDDFT level with and without coupling with the C 1*s* channels of the C_{60} cage. The fact that only a single curve is seen shows that the coupling has negligible effect.

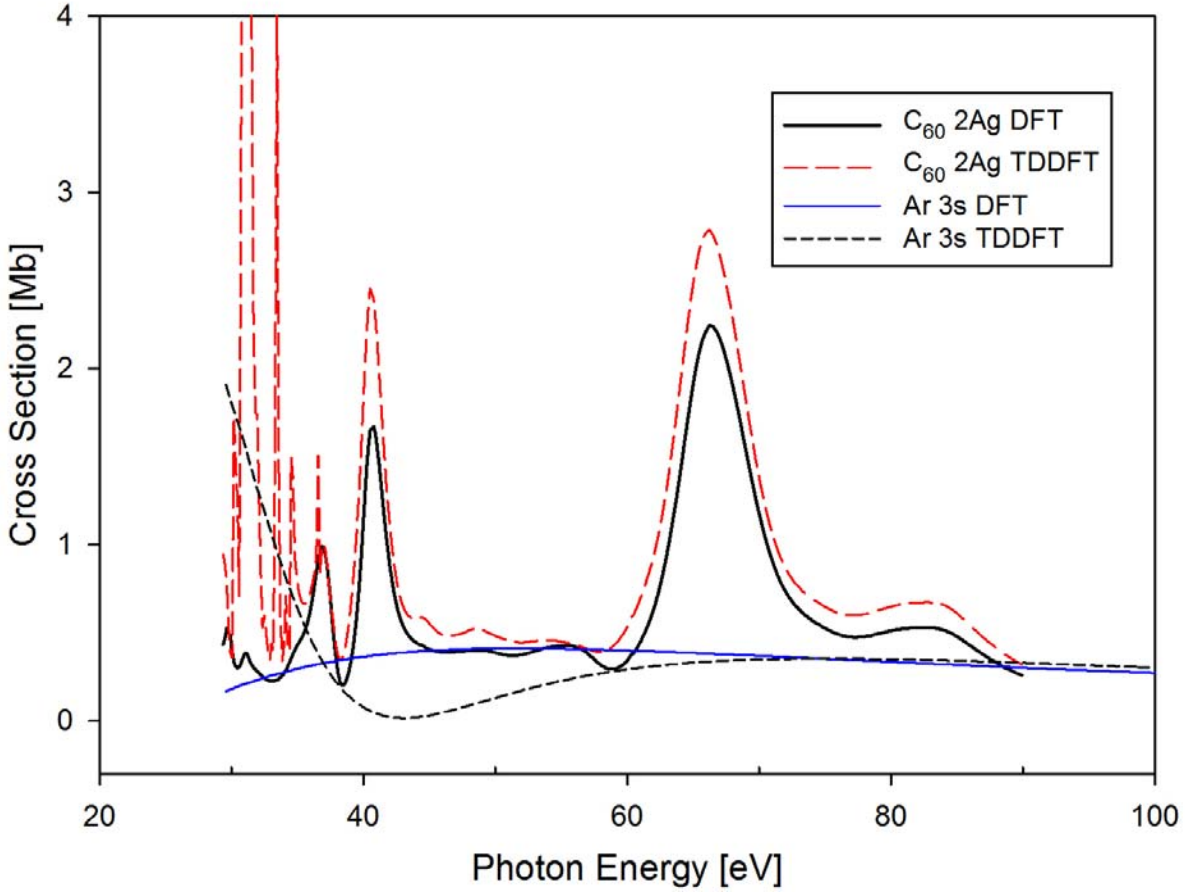

Fig. 3: (color online) Calculated photoionization cross sections for the free Ar 3s and the free C_{60} 2Ag states at both DFT and TDDFT levels of approximation.

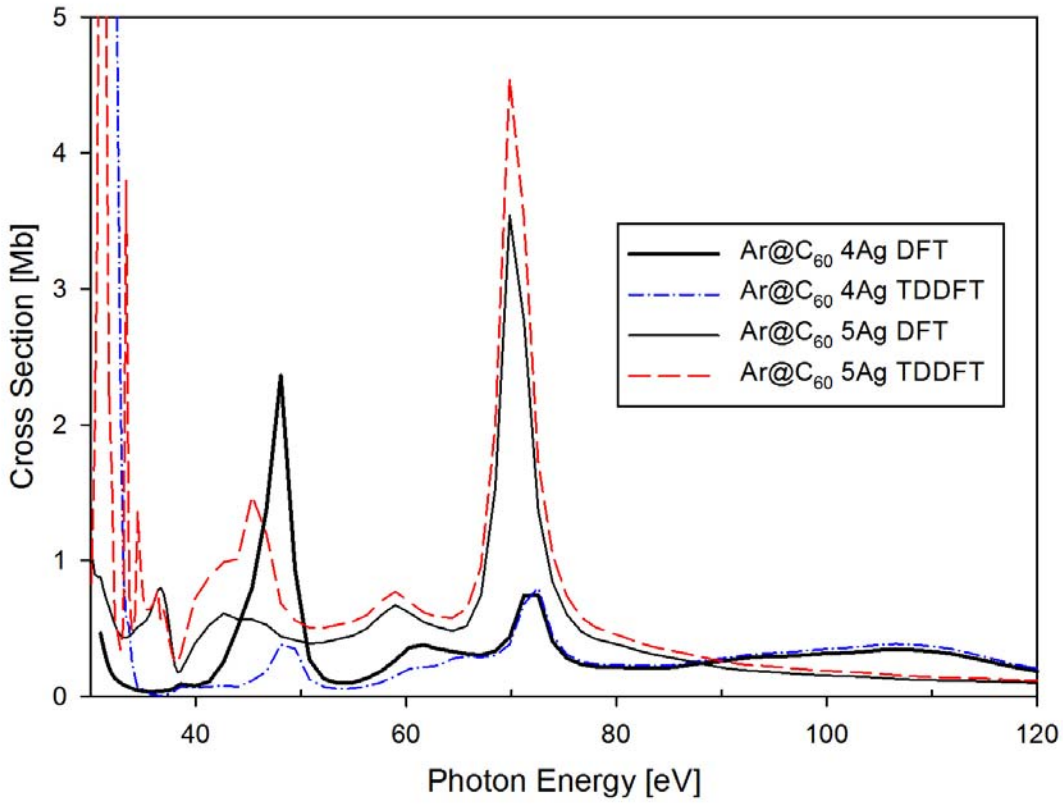

Fig. 4: (color online) Calculated photoionization cross sections of the 4Ag and 5Ag subshells of $Ar@C_{60}$ at DFT and TDDFT levels of approximation. The 4Ag state is essentially Ar 3s (which is not hybridized) and the 5Ag is almost exactly the 2Ag state of free C_{60}.